

Machine learning approach to the safety assessment of a prestressed concrete railway bridge

Original

Machine learning approach to the safety assessment of a prestressed concrete railway bridge / Marasco, Giulia; Oldani, Federico; Chiaia, Bernardino; Ventura, Giulio; Dominici, Fabrizio; Rossi, Claudio; Iacobini, Franco; Vecchi, Andrea. - In: STRUCTURE AND INFRASTRUCTURE ENGINEERING. - ISSN 1573-2479. - (2022), pp. 1-15.
[10.1080/15732479.2022.2119581]

Availability:

This version is available at: 11583/2971818 since: 2022-09-28T16:56:19Z

Publisher:

Taylor & Francis

Published

DOI:10.1080/15732479.2022.2119581

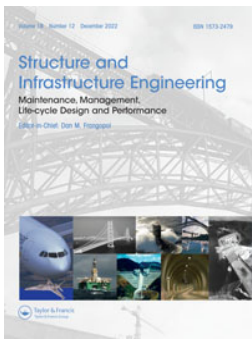
Terms of use:

openAccess

This article is made available under terms and conditions as specified in the corresponding bibliographic description in the repository

Publisher copyright

(Article begins on next page)



Structure and Infrastructure Engineering

Maintenance, Management, Life-Cycle Design and Performance

ISSN: (Print) (Online) Journal homepage: <https://www.tandfonline.com/loi/nsie20>

Machine learning approach to the safety assessment of a prestressed concrete railway bridge

Giulia Marasco, Federico Oldani, Bernardino Chiaia, Giulio Ventura, Fabrizio Dominici, Claudio Rossi, Franco Iacobini & Andrea Vecchi

To cite this article: Giulia Marasco, Federico Oldani, Bernardino Chiaia, Giulio Ventura, Fabrizio Dominici, Claudio Rossi, Franco Iacobini & Andrea Vecchi (2022): Machine learning approach to the safety assessment of a prestressed concrete railway bridge, Structure and Infrastructure Engineering, DOI: [10.1080/15732479.2022.2119581](https://doi.org/10.1080/15732479.2022.2119581)

To link to this article: <https://doi.org/10.1080/15732479.2022.2119581>



© 2022 The Author(s). Published by Informa UK Limited, trading as Taylor & Francis Group.



Published online: 26 Sep 2022.



Submit your article to this journal [↗](#)



View related articles [↗](#)



View Crossmark data [↗](#)

Machine learning approach to the safety assessment of a prestressed concrete railway bridge

Giulia Marasco^a , Federico Oldani^b, Bernardino Chiaia^a , Giulio Ventura^a , Fabrizio Dominici^b , Claudio Rossi^b , Franco Iacobini^c and Andrea Vecchi^c

^aDepartment of Structural Geotechnical and Building Engineering, Politecnico di Torino, Torino, Italy; ^bLINKS Foundation, Torino, Italy; ^cRete Ferroviaria Italiana (RFI), Roma, Italy

ABSTRACT

Early structural anomalies identification allows to hold maintenance activities that avoid loss of both economic resources and human life. This is extremely important for crucial infrastructures like railway bridges. This paper illustrates the structural health monitoring approach applied to a simply supported prestressed concrete railway bridge. In the framework of long-term monitoring, both static quantities (displacements, strains, and rotations) and environmental measurements (temperatures) have been recorded. Machine learning techniques, Extreme Gradient boosting machine and Multi-Layer Perceptron, have been exploited to build regression correlation models associated with the undamaged structural condition after adequate pre-processing operations. In this way, alarm thresholds based on the expected residuals between the predicted structural quantities and the measured ones, have been defined. The thresholds turned out to be able to catch early-stage anomalies not pointed out by traditional damage thresholds based on the design values. The proposed damage index is chosen as the moving median of the residuals, allowing a significant reduction of false alarms. The used correlation models and the obtained results represent a starting point for the generalization of this approach to the bridges belonging to the same static typology.

ARTICLE HISTORY

Received 11 November 2021
Revised 12 May 2022
Accepted 29 June 2022

KEYWORDS



Bridge maintenance; damage assessment; intelligent structures; prestressed concrete bridge; railway systems; structural control

1. Introduction

Railway bridges are one of the most crucial and critical parts of the worldwide infrastructural system. They are affected by degradation processes of different nature and duration (Bieñ et al., 2007). Changes in physical and/or chemical structural features due to incidental, short-time or long-time processes are often the causes of the structural malfunction or collapse. In Italy, the largest part of railway viaducts built starting from the second half of the 20th century is made of prestressed concrete simply supported bridges. Although these are simple structures and their reliability is proven, several degradation phenomena as fatigue, aging, and corrosion can evolve over time and reduce structural safety. Depending on the source of damage, some structural sections of the deck are more prone to undergo degradation. For instance, the corrosion phenomenon is more intense and spread in some sections localized near elements (e.g. joints, niches, and ducts) where both the presence of water and deicing salts is found. A structural analysis is fundamental to understand which parameters and sections have to be monitored. The consequent failure structural modes (Sgambi, Malerba, Gotti, & Ielmini, 2012) will depend on the type, position, and entity of the damage. In the worst case, shear failure mode can take over (Kamaitis

& Kamaitis, 1996) leading to sudden and brittle collapses. The changes of some structural features may be discerned through a variation of some measurable quantities, static (Inaudi, 2010; Nguyen, Schommer, Maas, & Zürbes, 2016) and dynamic, along with the structure.

Many studies have been carried out in the dynamic field (Azzara, De Falco, Girardi, & Pellegrini, 2017; Roselli et al., 2018, Peeters & De Roeck, 2001; Zhou & Yi, 2014; Magalhães, Cunha, & Caetano, 2009). In particular, the operational modal analysis technique (Ivanovic, Trifunac, & Todorovska, 2000; Magalhães & Cunha, 2011; Priori, De Angelis, & Betti, 2018; Rainieri & Fabbrocino, 2010) is widely used because, being output-only, it avoids the use of instrumentations to excite the structure and does not interfere with its operation. Among the recent and innovative studies using dynamic features for anomaly detection and condition assessment, it is worth focusing on (Arul & Kareem, 2020; Liu, Niu, Zhao, Duan, & Shu, 2022; Tang, Chen, Bao, & Li, 2019). They faced such task by detecting six types of anomalous data patterns (e.g. missing, mirror, outlier, square, trend, and drift). The first one uses a Random Forest classifier with a 'Shapelet transform'; the second one is based on Generative Adversarial Networks

CONTACT Giulia Marasco  giulia.marasco@polito.it  Department of Structural Geotechnical and Building Engineering, Politecnico di Torino, Corso Duca degli Abruzzi 24, 10129 Torino, Italy.

© 2022 The Author(s). Published by Informa UK Limited, trading as Taylor & Francis Group.

This is an Open Access article distributed under the terms of the Creative Commons Attribution-NonCommercial-NoDerivatives License (<http://creativecommons.org/licenses/by-nc-nd/4.0/>), which permits non-commercial re-use, distribution, and reproduction in any medium, provided the original work is properly cited, and is not altered, transformed, or built upon in any way.

(GAN) and Convolutional Neural Networks (CNN); the third one exploits a CNN for the image classification.

All methodologies show high accuracy; however, they may not be fully suitable for all scenarios (e.g. different structural typologies, materials, and recorded parameters). For example, in the one described in this paper, catching drift will not suffice because the occurrence could be caused by both anomalous phenomena and not. Much recent research has concentrated on stay cables condition assessment. Although several concepts can be identified as common elements of monitoring techniques, it's crucial to underline that customized approach are preferable for each structural typology. A technique is proposed by Zhang, Yan, Li, Pan, and Dong (2021). Starting from measured cable forces, the cable with the lowest classification accuracy is considered the most likely to be damaged. This method, which identifies the damaged structural part as the one that differs from its healthy state the most from the others, assumes many structural elements considered critical to be monitored. In the case of cable-stayed bridges, this is a meaningful methodology since cables, present in large numbers, play a key role. In the case under study in this paper, the structural typology shows limited critical sections in an optimization perspective. Consequently, the anomaly is identified no longer comparing the response of several elements but focusing on the single ones.

In addition to studies carried out in the field of dynamics, the literature presents, albeit on smaller scale, investigations rely on static measurements (Marasco, Piana, Chiaia, & Ventura, 2022; Tonnoir, Carde, & Banant, 2018). Advantages derived from their use include a higher degradation local sensitivity and easier damage localization (Chou & Ghaboussi, 2001). Furthermore, they are frequently simpler and more precise than dynamic ones (Jenkins, Kjerengtroen, & Oestensen, 1997). Focusing on strains data, model-based (Sanayei, Phelps, Sipple, Bell, & Brenner, 2012) and data-driven approaches have been developed. Cardini and DeWolf (2009) proposed a system, set to catch the passage of trucks, using high frequency recorded strain data. It determines live load stresses, load distribution factors, and neutral axis position in healthy conditions as a benchmark for structural assessment. Such interesting approach is not applicable to the case study described here, as the latter uses a considerably lower sample rate to optimize and store data over time. Similarly, albeit differently, Bao et al. (2019) proposed to capture the structural response to load passage and not the one to environmental factors for a steel girder assessment.

On the other hand, time series strain data have been used for mapping the strain responses with temperature. Duan, Li, and Xiang (2011) use a linear regression model for such task for a tied arch bridge built 14 years before the monitoring system installation. As a result, time-delayed structural phenomena are absent, and pre-processing techniques are not required, as in present study. In (Ding, Wang, Sun, Wu, & Yue, 2015) correlation models between temperature and static strains of a steel truss arch bridge have exploited to define the healthy condition for damage detection purposes. Also in this study, time-delayed phenomena

are negligible and there are no strategies required to ensure data repetition. To a complete up-to-date overview, the use of CV and ML-based methods have to be mentioned (Bao & Li, 2021). Although they can detect multipattern anomalies of SHM data efficiently with high accuracy, their applications are limited as they are related to the presence of extreme condition and damage data.

As clear from the studies reported so far, the need to develop reliable systems with good accuracy and short detection time, to control the structural safety for an effective data-driven decision-making operation and maintenance (O&M) of bridges (Wu et al., 2022) is nowadays pressing. The development of new monitoring strategies (Chiaia, Ventura, Zannini Quirini, & Marasco, 2019; Chiaia, Marasco, Ventura, & Zannini Quirini, 2020) and the advances both in traditional methods and in machine learning applications (Avci et al., 2021; Civera, Zanotti Fragonara, & Surace, 2020) represent the scientific tools to tackle this challenge for engineers, researchers, and infrastructure owners. Railway bridges specifically for high-speed trains, are object of considerable attention by infrastructure owners due to the possible tragic consequences that a structural malfunction could provide. The RFI (Rete Ferroviaria Italiana) company has developed an automatic monitoring system, whose modularity (Ding et al., 2015) has involved the need of several expertise, with the aim to control the performance of a series of railway bridges.

The present study focuses on the last phases of the whole SHM system process, namely on the data analysis and the evaluation of structural safety. Regression correlation models able to describe the structural undamaged behavior have been developed by using the data recorded in the first service years of the high-speed railway Brescia-Treviglio in northern Italy. To increase the accuracy of the models, two techniques have been utilized. The first belongs to data normalization techniques. As is well known, data normalization techniques are one of the essential pre-processing phases. Min-Max, Z-score, and Decimal Scaling stand out among the traditional normalization methods to be able to improve the machine learning models accuracy (Al Shalabi, Shaaban, & Kasasbeh, 2006; Nawi, Atomi, & Rehman, 2013; Obaid, Dheyab, & Sabry, 2019). However, they are often inefficient due to the non-stationarity of the time series (Ogasawara et al., 2010). For such reason, a sliding window technique has been exploited as a pre-processing operation. It can filter out the impact of some structural phenomena deferred in time, e.g. fluage. The problem at hand involves in continuous analysis of real-time data.

For this reason, for each new data, a z-score normalization is used in this study, based on the mean and standard deviation computed over the immediately previous fixed-time window. If the time size of the window is properly chosen, this approach allows to obtain stationary series within the desired range (Ogasawara et al., 2010). The second technique is the use of additional temporal features (e.g. the week of the year and the hour of the day associated with the recording time of the other features) to mitigate the lack of some environmental parameters (e.g. irradiation). Once created, the models have been utilized to set alarm thresholds for the infrastructure



Figure 1. View of the Oglio Viaduct.

control. To this aim, techniques in the field of machine learning and deep learning have been used. This approach, owing to the combination of several techniques, turns out to be actually fit for the case study at hand and allows to exploit the data to obtain a so-called ‘intelligent control’. The use of the data-driven alarm thresholds showed a greater ability to detect early-stage anomalies compared to thresholds based on the design values.

2. The structure of the bridge

The Oglio Viaduct, a railway bridge located in the northern of Italy nearby the highway A35 BreBeMi, has been the subject of the analysis. It allows the passage of the railway line above the homonymous river. It belongs to the high speed-high capacity rail route Brescia-Treviso, one of the segments of the Mediterranean Corridor that will connect the Western and Eastern Europe. It is 1287 meters long and it is composed of 43 spans, each of about 30 meters. A general view of the bridge is shown in Figure 1. Each bridge span is simply supported by the piers and is a grillage with four longitudinal 2.5 meters high prestressed beams and five diaphragms. The top slab shows two overhangs with service pathways. The track spacing, the beam spacing, and the beam width are 4.5, 2.6, and 2.56 meters, respectively. The prefabricated beam weight is 1219.48 kN. Each longitudinal beam is prestressed with 88 strands of 0.6-inch diameter (30 strands neutralized at the supports) and has a non-perfectly uniform profile due to section widening near the support. Its cross-sectional area is 1.2824 m^2 for approximately 90% of its length. The concrete beam’s Young’s modulus is about $36.28 \times 10^9 \text{ N/m}^2$. The piers of the viaduct have a 4 meters diameter circular shape connected at the top with a pier cap on which the spans are resting on. The foundation pile caps are laid underground to avoid scouring at the base. The elevation view of the span between the viaduct pier 3 and 4 is displayed in Figure 2.

3. Description of the SHM system

A long-term structural health monitoring system has been designed and installed on the Oglio Viaduct by Rete Ferroviaria Italiana. Its main aim is to highlight the temporal evolution of the bridge under environmental conditions by means of static measurements and to provide warnings for anomalous values of monitored parameters. It

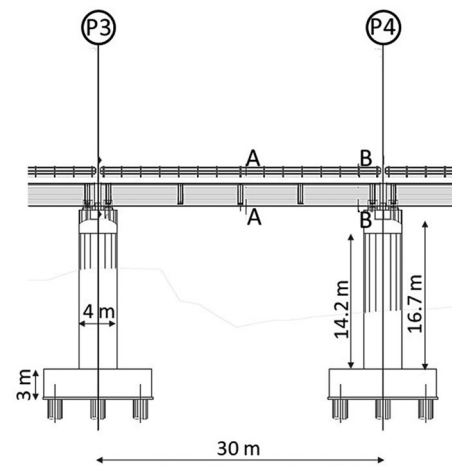


Figure 2. Elevation view of the viaduct.

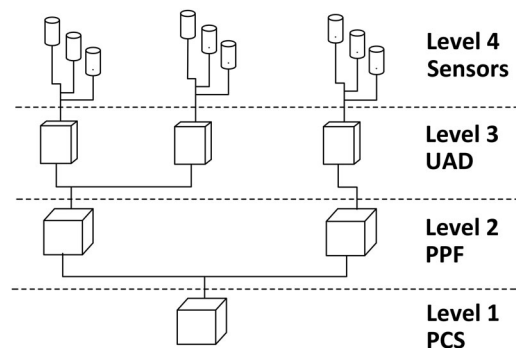


Figure 3. Monitoring system architecture.

is not designed to capture the effects of train transit because its objective is not to capture the structural response corresponding to operation loads that would require high signals sampling rate. Sensors, typically strain gauges, displacement meters at supports, clinometers, surface and air thermometers have been used to measure key parameters in different sections of the structure. They constitute the labelled Level 4 in the hierarchical monitoring plan shown in Figure 3. The highest levels of hierarchy are as follows: the UAD (Data Acquisition Unit), the PPF (Fixed Peripheral Places) and the PCS (Satellite Central Place).

After system installation, the data acquired from sensors have been compared in real-time with expected values set by experts in structural monitoring and design thresholds (DT) have been defined. The additional step, developed and presented in this paper, is the definition of regression correlation models describing the real structural behavior to define data-driven undamaged condition thresholds (UCT).

4. Sensors network and methodology

The structure, in service for about six years, was tested by means of modular railway cars with a maximum axle load of 40 tons to reproduce the maximum action to which the viaduct can be subjected. Furthermore, the railway superstructure was tested using diagnostic trains with a speed of 300 km/h. During its life, the viaduct is regularly checked both in the railway superstructure with diagnostic trains and

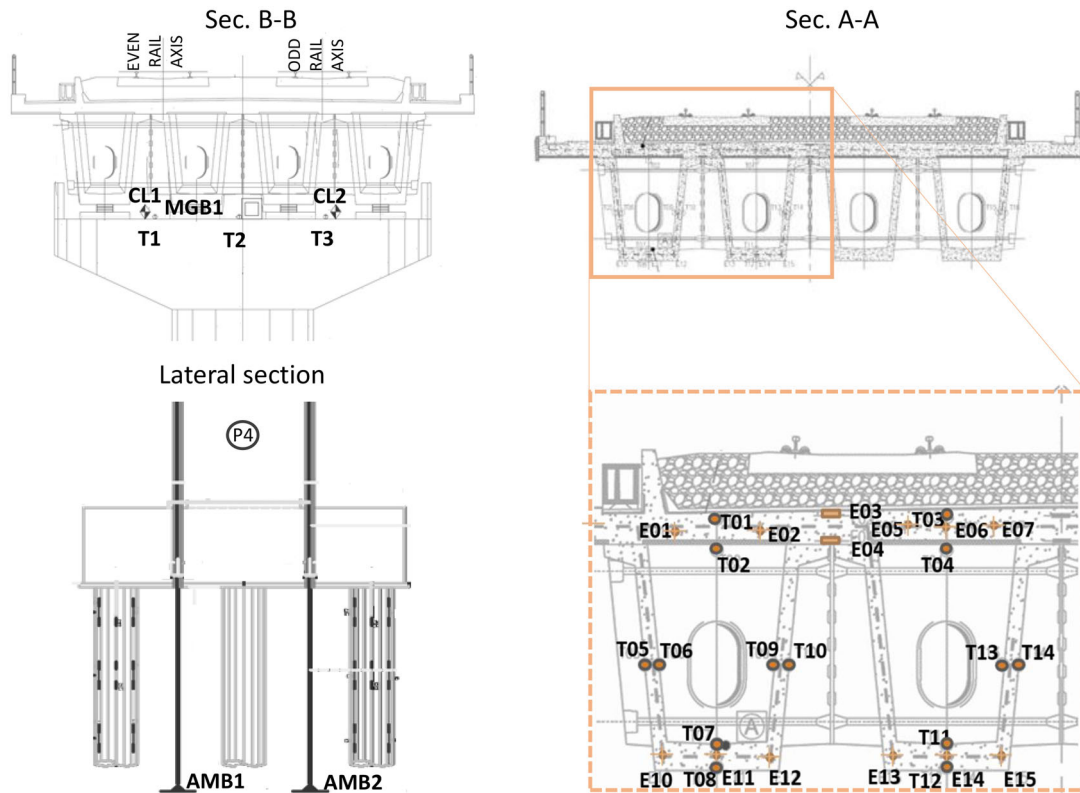


Figure 4. Sensors network.

Table 1. Symbols.

Symbol	Sensor
T	Thermometer (temperature of the material or of the air)
E	Strain gauge
CL	Clinometer
MGB	Biaxial support displacement
AMB	Single-base Measurer of settlement

with visual inspections. Evidence from periodic and additional checks are conveyed to the information system Domus-Inrete 2000 that controls and reports the structural state as well. Due to the absence of the reported structural anomalies, the data recorded on the structure have been associated with an undamaged structural condition.

The data exploited for the development of the correlation models (Figure 4) have been recorded in two meaningful sections for the structural typology: A-A (midspan) and B-B (support), Figure 2. Table 1 reports the symbols labelling the sensors. The sensor data have been processed with the novelty detection approach presented in (Al-Dahidi, Baraldi, Di Maio, & Zio, 2014; Hu, Palmé, & Fink, 2017). The choice to perform the analysis with this technique is justified by two reasons. Firstly, real data belonging to the damaged structural condition are not available. Secondly, the generation through simulation of damaged structural data can be not fully reliable in terms of types of potential structural anomalies. In fact, if a classification model had been trained to recognize only some types of anomalies, the system may not be able to catch other types. Consequently, the models aim to highlight anomalies of any nature and there is no classification of the damage type.

The adopted approach is based on the training of machine learning regression models on a data set belonging to the health conditions, so to learn what are the correlations between quantities selected as independents (inputs) and the ones selected as dependents (outputs). The selection of independent and dependent parameters is based on cause-and-effects relationships rooted in physical phenomena. Once trained, these models are validated using another set of data for the undamaged structure (the error validation set). From the inputs of such dataset, the model predicts the outputs, and it is possible to compute the error (residual) in terms of the difference between the measured and the predicted outputs. In this way, the window of error dispersion is defined through its mean (μ) and its standard deviation (σ). It represents the 'healthy condition error range' and its extremes are defined by the expression $\mu \pm k\sigma$, where k represents a *controlling parameter*. The extremes of the 'healthy condition error range' correspond to the undamaged condition-based alarm thresholds (UCT). The alarm thresholds UCT, developed using the above-mentioned methods, reflect the undamaged structural condition and depend strongly on the parameter k whose value is chosen, according to the type of problem, from a range of statistically significant values. The value of k used ranging from 2 to 3. In this way, the probability of having false alarms varies from 5 to 0.3%. Values out of this range should be reported as anomalies.

If the residual had been considered as damage index, as in the classical signal reconstruction approach, lots of false positives would be present. To overcome this problem, the moving median of the residuals with respect to the seven preceding days has been adopted as such. In this way, if at

least more than 50% of the signals in the previous week have an error falling outside the threshold, an anomaly is reported. Seven days are considered a large enough time to filter out false alarms and small too to report anomalies in time. This technique is a particularly strong filter for reducing false positives in cases of residuals oscillating in sign beyond the defined thresholds, under specific conditions. This damage index allows to smooth the peaks of the residual providing structural health monitoring more effective for actual use owing to the reduction of maintenance costs.

It is worth pointing out the method used in the pre-processing phase, consisting of a z-score normalization with respect to a moving time window. Among the most common data transformation normalization approaches are the min-max, the z-score, and the decimal scaling. Of them, the z-score method overcomes the limitation of knowing the minimum and maximum value of the series but can only be applied to stationary series. As in other fields, e.g. finance and economics, most time series associated with structural quantities are non-stationary (Tsay, 2005). This behavior is accentuated for some materials such as concrete that develop phenomena deferred in time (e.g. fluage). To effectively handle non-stationary problems, a sliding window technique has been adopted. In this specific case, the values (v), for input and output time-series, have been normalized with the following formula (Equation (1)), where μ and σ are the mean and standard deviation computed on the data belonging to the previous temporal window, respectively. After the introduction of the normalized value v' in the machine learning algorithm, the data have been rescaled in their original range (Equation (2)) by means of a post-processing operation consisting of an inverse z-score normalization:

$$v' = \frac{v - \mu}{\sigma} \quad (1)$$

$$v = \sigma v' + \mu \quad (2)$$

More details are given in Section 5.

5. Correlation models

Starting from the data collected in the first service years of the structure, three regression correlation models have been developed to control the following aspects: the strains of the unloaded deck, the displacements and the rotations of the piers, and the deck-support displacement with respect to environmental conditions. Several machine learning techniques (e.g. Extreme Gradient Boosting Machine, Multi-Layer Perceptron, LSTM, Bayesian Ridge Regressor) have been studied for each problem. The problems are expressed as regression models, as anticipated, due to the continuous nature of the values and are designed to correlate inputs and outputs measured at the same time, and not to predict outcomes at later instants. Those producing the best regression model, in terms of Mean Absolute Error and Symmetric Mean Absolute Percentage Error on the error validation set, have been selected and shown in the following sections. Such techniques have been proved to be extremely efficient for two of the three tasks (Section 5.1. and 5.2.). A much simpler

approach has been adopted for the assessment of pier displacements due to its linearity. For such reason, it is not reported in this study. In the following a brief description of the models that have shown the best results is reported.

The first model is the Extreme Gradient Boosting Machine (XGBoost). The term 'Boosting' refers to a family of algorithms which converts weak learners to strong learners. Boosting is an ensemble method for improving the model predictions of any given learning algorithm. It is usually used with a Decision Trees ensemble. Decision Tree classifies data into branch-like segments that construct an inverted tree with a root node, internal nodes, and leaf nodes (Quinlan, 1986). The algorithm is non-parametric and can efficiently deal with large, complicated datasets without imposing a complicated parametric structure. It uses the training dataset to build a decision tree model and a validation dataset to decide on the appropriate tree size needed to achieve the optimal final model. Gradient Boosting works by sequentially adding predictors to an ensemble, each one correcting its predecessor trying to fit the new predictor to the residual errors made by the previous predictor. XGBoost is a specific implementation of the Gradient Boosting method which delivers more accurate approximations by using the strengths of second order derivative of the loss function, L1 and L2 regularization and parallel computing. XGBoost is particularly popular because it demonstrated to solve regression and classification problems in a more optimized way than other machine learning techniques (Chen & Guestrin, 2016).

The second model is the Multi-Layer Perceptron (MLP). It is a class of feedforward artificial neural networks able to model extremely complex functions. Originally proposed by McClelland, Rumelhart, and Hinton (1986), Multi-Layer Perceptron consists typically of artificial units that receive several inputs from input data or from other units in the neural network. Each unit performs a weighted sum plus bias and passes through an activation function that is composed of a nonlinear function (Equation (3)), where y is the output of the MLP neuron, f is the activation function, W is the set of weights in the layer, x is the input vector and b is the bias vector). An example of popular activation function is Relu (Equation (4)). The produced output is then passed to another unit of the successive layer of the net. With a defined number of layers and number of units in each layer, the network's weights and thresholds must be set to minimize the prediction error made by the network defined through the loss function. This is the role of the training algorithms which use iterative techniques called stochastic gradient backpropagation:

$$y = f(Wx + b) \quad (3)$$

$$f(x) = \max\{0, x\} \quad (4)$$

5.1. Assessment of the midspan strain of the unloaded deck

5.1.1. Problem definition and data analysis

The evaluation of the strain state of the deck is fundamental to prevent some structural problems. Indeed, the

Table 2. Input and output parameters for correlation model.

INPUT	OUTPUT
Air temperatures (T1, T2, T3)	Strains at intrados of the midspan section
Mean _{ET} =mean [T01, T02, T03, T04]	
Mean _{IT} =mean [T7, T8, T11, T12]	
Tot _G = Mean _{ET} - Mean _{IT}	
E _G =mean [T01, T02]-mean [T7, T8]	
I _G =mean [T03, T04]-mean [T11, T12]	
[T01-T02]	
[T03-T04]	
[T7-T8]	
[T11-T12]	
Additional temporal features	

deformations are the mirror of potential cracks or pretension losses. Studies in the literature (Gonzales, Ülker-Kaustell, & Karoumi, 2013) have highlighted how, even the change of just one factor (e.g. temperature) leads to changes in structural properties expressible through non-linear laws. For example, structural stiffness increases dramatically when the temperature is less than zero degrees Celsius, and this is captured through pronounced increases in natural frequencies. Due to the complexity of the problem, the use of deep learning techniques to build undamaged structural models turns out to be effective.

The exploited parameters to develop the correlation model in the undamaged condition have been the ones recorded in the midspan section (Table 2). The first step to build a correlation model that links the strain values to factors that cause them in healthy structural conditions, based on the specific monitoring system, has been the identification of the independent parameters. The strain data are due to four factors: temperature, temperature difference (gradient), piers rotations, and train transit. The last factor has been left out, despite, as revealed by fairly recent studies (Matsuolka, Tokunaga, & Kaito 2021), the effect of the crack is maximum at the passage of loads making it possible to accurately predict the immediate drop in stiffness. Such choice is due to several reasons. The strains due to high-speed trains are characterized by high frequency and are lower in magnitude than the ones caused by absolute temperature and gradient of temperature (Ding et al., 2015).

Besides the monitoring system, as described in Section 3, is not designed to measure the effects of the passage of trains, the recordings having been done every 2 or 4 hours. The development of the monitoring system architecture is part of an overall optimization perspective. The proposed methodology, even without the amplification of instantaneous reduction of stiffness due to the transit of trains, can pick up quite small signal changes. Future developments may however foresee the introduction of this component to detect smaller anomalies. The contribution of piers rotations has also been neglected. This is due to the lower quantity and quality of available data. Three types of input can be distinguished: raw, processed, and additional input. The term raw points out the readings at the sensors without any elaboration (e.g. air temperature). The term processed is used for the input obtained after the processing of several raw inputs (e.g. mean sensor data). The term additional is utilized for features not directly linked to the readings at

sensors. In detail, reference is made to additional temporal features indicating the hour of the day (Equations (5) and (6)) and the week of the year (Equations (7) and (8)) in which the parameters were recorded. To feed the model with time information, those features have been encoded using sine and cosine functions of the values to ensure time data continuity and periodicity as follows:

$$h_s = \sin\left(2\pi \cdot \frac{h}{24}\right) \quad (5)$$

$$h_c = \cos\left(2\pi \cdot \frac{h}{24}\right) \quad (6)$$

$$w_s = \sin\left(2\pi \cdot \frac{w}{52}\right) \quad (7)$$

$$w_c = \cos\left(2\pi \cdot \frac{w}{52}\right) \quad (8)$$

The values of the hours (h) are within the range [0–24], the ones of the weeks (w) within the range [1–52]. Using Equations (5) and (6) for hours and Equations (7) and (8) for weeks, the system can uniquely identify these two parameters. Figure 5 displays the sine and cosine representing the 24 hours of the day and an illustrative example of the values (h_s and h_c) obtained for a specific hour of day (e.g. 10 a.m.). For the outputs of the system, only raw outputs have been utilized. Figure 6 displays the trends of the input-output data.

From a structural point of view, it is interesting to examine the evolution of the strain over time. As expected, there are large fluctuations in time at seasons change. Moreover, the seasonal effects of the thermal inertia of the deck (e.g. the effects of a hot summer are reflected until the early autumn periods) emerge observing the trend of strains that is like a sawtooth wave. In fact, the trend of the strain is roughly opposite to the one of the temperatures but after time intervals in which the temperatures are enough high (summer), the reduction of strains is manifested with a very slight downward trend, almost constant. Thus, under the same temperature, the observed strains in autumn are lower than the ones recorded in spring. This is the reason for which the temporal features, to identify the hour of the day and the week of the year, have been added as inputs of the correlation model. Certainly, in addition to the temperature effects, there are additional ones deferred over time: shrinkage and creep (Guo, Sause, Frangopol, & Li, 2011; Li et al., 2019; Liverani, n.d.). They explain the decreasing trend of the strains. Besides, other complementary effects as the ones due to non-ideal mobile supports and to drift over time of the sensors should be considered, but they are quite often of very difficult determination.

5.1.2. Model and pre-post processing operations

A pre-processing operation consisting of a z-score normalization, for input and output time-series, w.r.t. the preceding 60 days has been performed. The duration of normalization period has been chosen to take into account the data seasonality. This has allowed to filter the data deleting the effects that precluded their repetitiveness in time. As can be

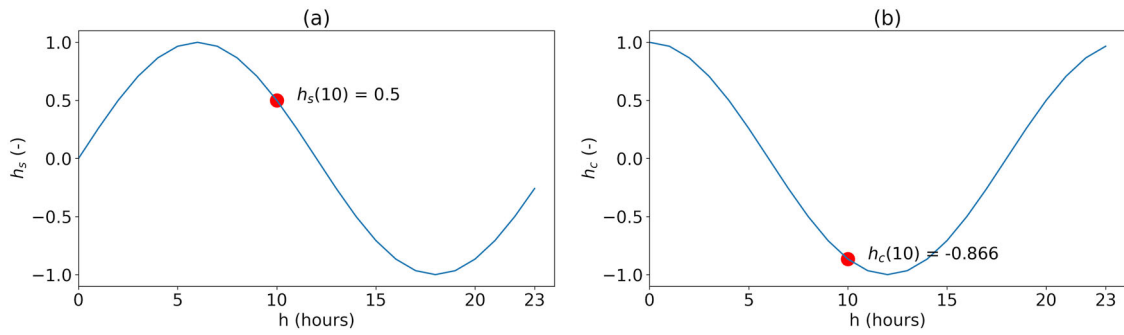


Figure 5. Functions to obtain the additional temporal features (e.g. hour of the day). a Sine function; b Cosine function.

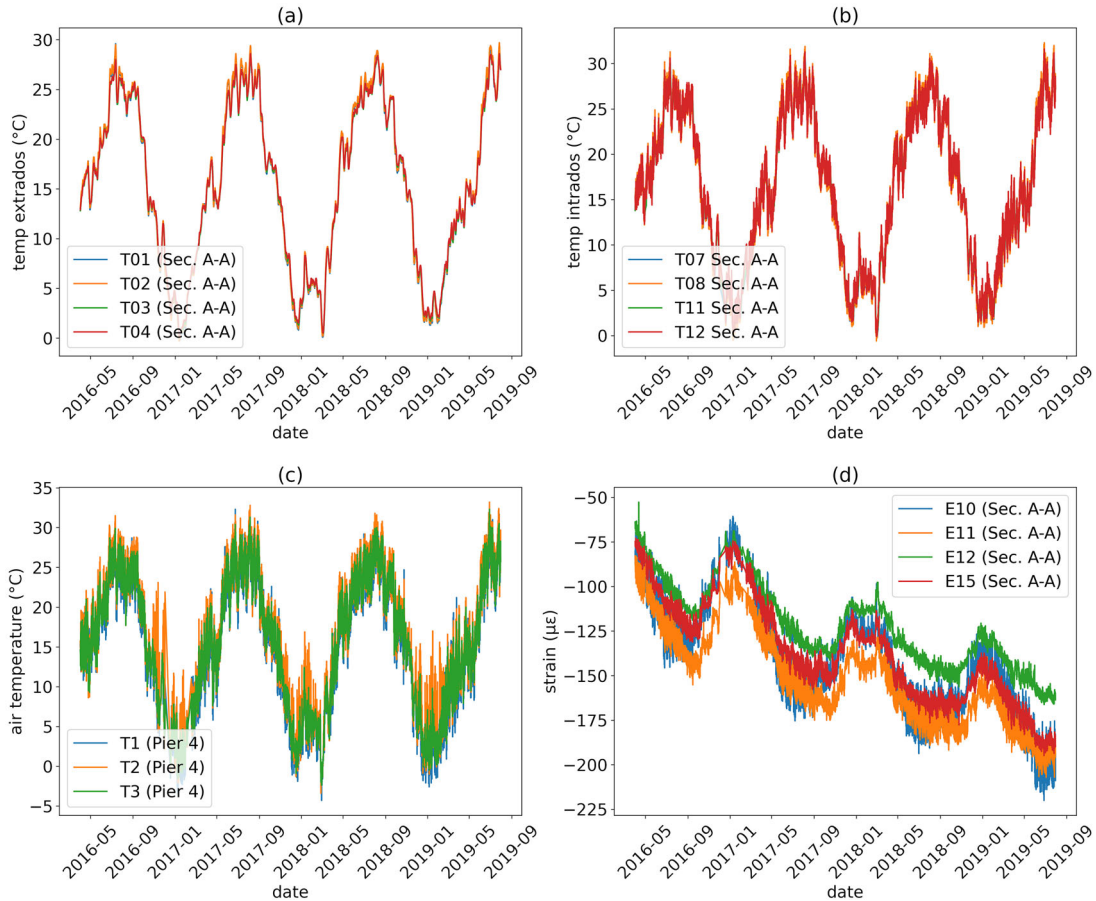


Figure 6. Input and output parameters for correlation model. a Temperature extrados; b Temperature intrados; c Air temperature; d Strain.

seen in Figure 7, it was possible to obtain a stationary time series using the moving window normalization.

Several supervised learning algorithms have been adopted as regression models. As described in the introduction of the Section 5, two of them (Extreme Gradient Boosting machine and Multi-Layer Perceptron) have achieved the best results. In detail, the Extreme Gradient Boosting model (Chen & Guestrin, 2016) was set with decision trees with a maximum depth of 6. The Gradient Boosting technique, with a learning rate of 0.3, has been used to increase the model accuracy. The Multi-Layer perceptron, instead, was composed of two hidden layers of 30 and 20 neurons, respectively. The Mean Square Error (*MSE*) has been used as criterion and the Adam algorithm has been employed as optimizer. The learning rate was set to 0.001 and the maximum number of epochs to 400, the batch size is equal to

16. Then, the data have been rescaled in their original range by means of a post-processing operation consisting of an inverse z-score normalization.

Figure 8 displays the values of the strain over time and the subdivision of the overall set in three parts: train (50%), validation error (20%), and anomaly test (30%). As explained in Section 4, once the model has been trained, the validation error set has been exploited to compute the mean and the standard deviation of the residual useful to define the healthy condition error range by means of the UCT thresholds. The residual is calculated in terms of the difference between the measured (x_r) output after the post-processing operation, and the predicted (x_p) one. Table 3 reports the values of three indices obtained by the validation error set, for both the Extreme Gradient Boosting Machine and the Multi-Layer Perceptron, to evaluate the model accuracy. In detail, the used indices are:

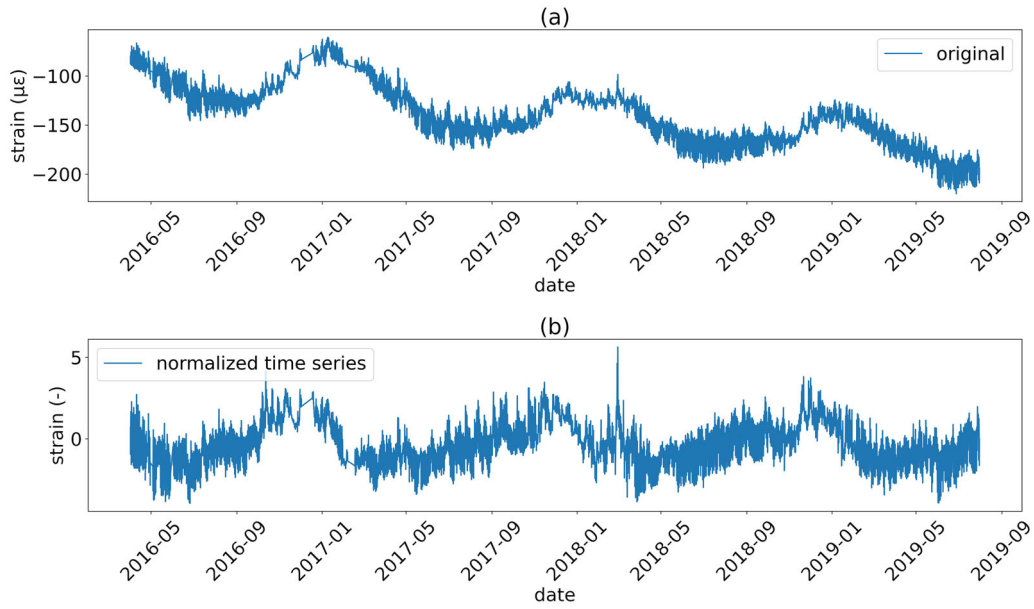


Figure 7. Signal E15 **a** original series; **b** normalized series.

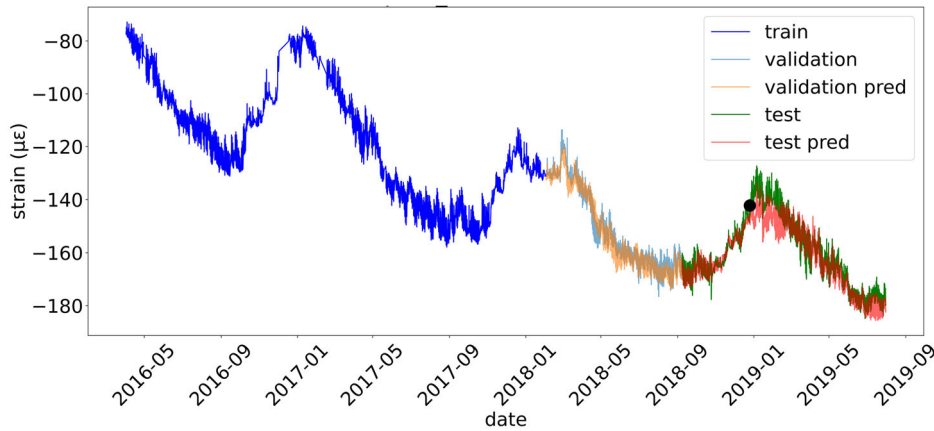


Figure 8. Strain. Signal E15. Subdivision into train, validation error and test anomaly set.

MAE (Mean Absolute Error), *SMAPE* (Symmetric Mean Absolute Percentage Error) and R^2 (Coefficient of determination). They are useful to quantify the reconstruction accuracy and have been utilized to choose which signals have been better predicted. Higher model performance is associated with low *MAE* and *SMAPE* values and high R^2 values. Their formulations are given in Equations (9) (10), and (11):

$$MAE = \frac{1}{n} \sum_1^n abs(x_p - x_r) \quad (9)$$

$$SMAPE = \frac{\sum_1^n abs(x_p - x_r)}{\sum_1^n (x_p + x_r)} \quad (10)$$

$$R^2 = 1 - \frac{\sum_1^n (x_p - x_r)^2}{\sum_1^n (x_r - \bar{x})^2} \quad (11)$$

In such formulations x_p is the predicted value, x_r the measured (real) one, and \bar{x} the average of the values.

The gradient boosting technique, by means of the combination of several decisional trees, has achieved better results in

Table 3. Models evaluation metrics (validation error set).

Sensor	MLP			XGBOOST		
	MAE ($\mu\epsilon$)	SMAPE (%)	R^2 (-)	MAE ($\mu\epsilon$)	SMAPE (%)	R^2 (-)
E10	3.560	1.046	0.794	3.022	1.020	0.965
E11	2.956	0.844	0.667	2.217	0.770	0.951
E12	1.744	0.613	0.764	1.545	0.610	0.97
E15	1.829	0.558	0.701	1.879	0.600	0.966

average both with respect to the Multi-Layer Perceptron and to other regression models (e.g. LSTM, Bayesian Ridge Regressor). These latter ones were not described in this article due to the worse results. The subsequent analyses have been focused on the sensors that have shown a Coefficient of determination close to 1 (greater than 95%). A scatter plot reporting the predicted and the actual values, from one of these sensors (E15), has been displayed in Figure 9 to visualize the goodness of the prediction.

5.1.3. Simulation of anomalies and damage identification

Simulated anomalies have been adopted to assess the damage identification capacity of the proposed approach. They

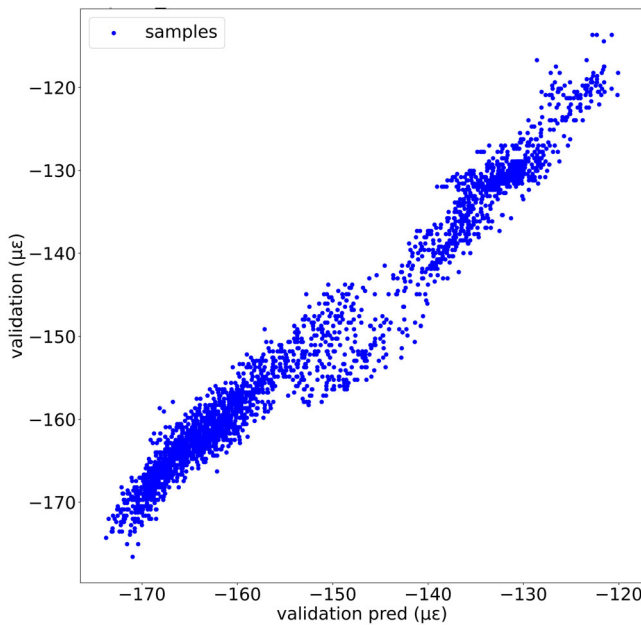


Figure 9. Scatter plot E15 (validation set).

have been simulated imposing a given offset in sensor values. This offset starts from zero and increases linearly in time up to the given value in three considered different time spans (168 h, 336 h, and 720 h). Each anomaly is therefore characterized by two parameters: the amplitude (offset) and the time span to reach the given offset. The reliability of the proposed strategy has been tested by varying the starting point of the anomaly. Fifteen points belonging to the test anomaly set have been considered. An illustrative example has been reported in Figure 10. The anomaly plot (Figure 10a) shows the application of an anomaly, on the signal of the sensor E15, by means of the imposition of an offset equal to $10 \mu\epsilon$ achieved in 168 hours. The black dot indicates the starting point of the disturbed signal. Figure 10b shows a zoom on the test set to highlight the largest difference found between the signal and its prediction near the starting point of the anomaly. On the other hand, the residual plot (Figure 10c) displays, for the test anomaly set, the trend of the residual (red line), the damage index (median), and the 'healthy condition error range' (orange band) limited by UCT thresholds. The residual error, expressed as difference between the measured output after the post-processing operation and the predicted one, has a Gaussian distribution with a mean close to the zero value. The value of k , for the sensor E10, E11, E12, and E15, to define the extremes of normality range (UCT) has been set equal to two. In the residual graph, the blue dashed circle indicates the identification of the anomaly. In that section the damage index falls beyond the control limit of the healthy condition error range.

Table 4 synthesizes the results in terms of detected anomalies, expressed by means of the ratio between the number of detected anomalies and the total number of anomalies tested equal to 15, as function of their amplitude and of the time span. The method successfully captures anomalies representing approximately 10% of the average signal value. Obviously, very

small anomalies that evolve in a wide time span are very difficult to detect. Beyond the ability to capture anomalies, it is important to note the absence of false positives. These were not detected for all sensors, except E11. For this sensor, there is a systematic error most likely due to high uneven local volatility (heteroscedastic time series). The results, expressed in percentage terms, may reflect good, mediocre, or poor damage detection capacity. The range of percentages and the colour associated with each of these definitions is given in the table caption.

The ability of the undamaged condition-based thresholds (UCT) turned out to be greater with respect to the design-based thresholds (DT) in detection of early-stage anomalies. These are established based on considerations resulting from the expected structural response. The design alert values are set equal to 100% of the calculation value chosen as the limit based on the maximum stresses obtained in the service phase. The alarm values are equal to 120% of this limit value. In detail, the design defines alert and alarm thresholds equal respectively to $103.5 \mu\epsilon$ and $124.2 \mu\epsilon$ for the sensors E10, E11, and E12. The corresponding thresholds for the sensor E15 are set equal to $230.25 \mu\epsilon$ and $276.3 \mu\epsilon$. Being the detected anomaly by the UCT of the order of $10 \mu\epsilon$, the gain in terms of detection capacity attainable using this approach is clear. Figure 11 shows a comparison between the two approaches by simulating an anomaly with an offset of $15 \mu\epsilon$ and a time span of 168 h on the signal recorded by the sensor E15. As visible, this anomaly (disturbed signal plotted in violet) would not be signaled by the design-based thresholds (DT). Indeed, the red and yellow horizontal lines that indicate the alarm and alert thresholds based on design are above the damaged/disturbed signal. On the other hand, the latter exceeds the thresholds defining the healthy condition error range, namely the UCT. Thus, the data-driven approach results more effective.

5.2. Assessment of pier rotations and joint expansion

5.2.1. Problem definition and data analysis

The assessment of the pier rotation and deck-support displacement is crucial to understand the presence of irregular piers movements and abnormal motions in the deck plane. Correlation models for the undamaged condition have been developed starting from the consideration that, in unloaded structural condition, clinometers and measurement of deck-support displacement are the mirror of the temperatures. Such models utilize as input the average air temperature, the rotations recorded by the clinometers, and the hour of the day corresponding to the recorded parameters. The exploited parameters to develop the correlation models in the undamaged condition have been reported in the Table 5.

More specifically, clinometers CL1 and CL2 (Figure 4) have two channels defined by the abbreviations CL_CHA and CL_CHB that refer to the rotation in the longitudinal and transverse directions, respectively. Due to poor signal quality, recordings of channel CL1 CHA were not considered as model input. Figure 12 shows the behavior of the longitudinal rotation measured by the sensor CL2 CHA. On

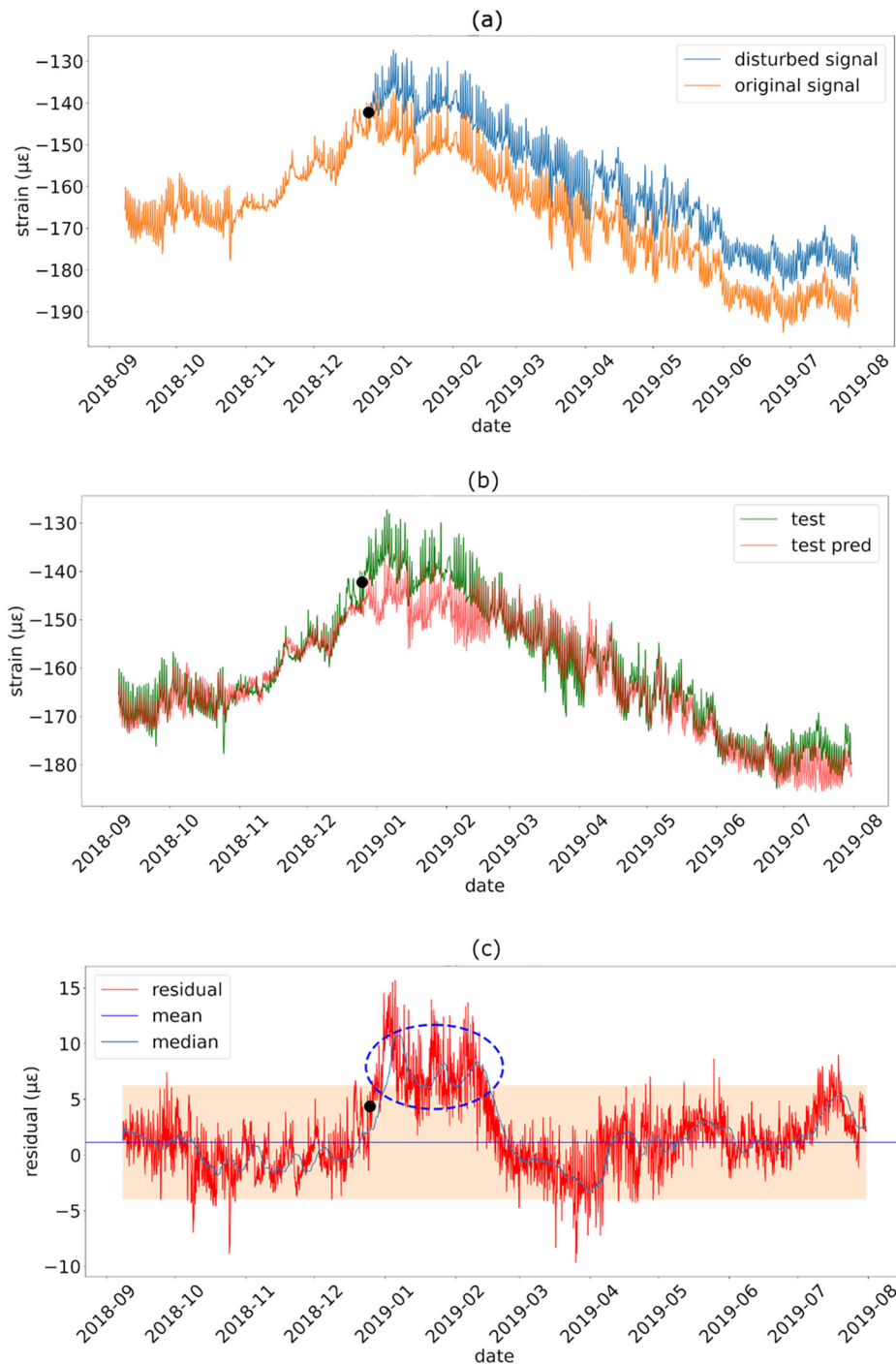


Figure 10. **a** Anomaly plot; **b** Test set; **c** Residual plot.

the other hand, the output are the measurements recorded by the biaxial joint gauges. Figure 13 displays the trend in time of the signals recorded by the sensors MGB1L (longitudinal) and MGB1T (transversal) and the subdivision of the overall set in three parts. It should be noted that from an engineering point of view the two sensors are different. The first measures the displacement of the deck to the support in the direction of the viaduct axis. The second one in the transverse direction. The latter shows measurements with a very small range of variation due to the layout of the constraints on the internal beam supports which block transverse displacements.

5.2.2. Model and pre-post processing operations

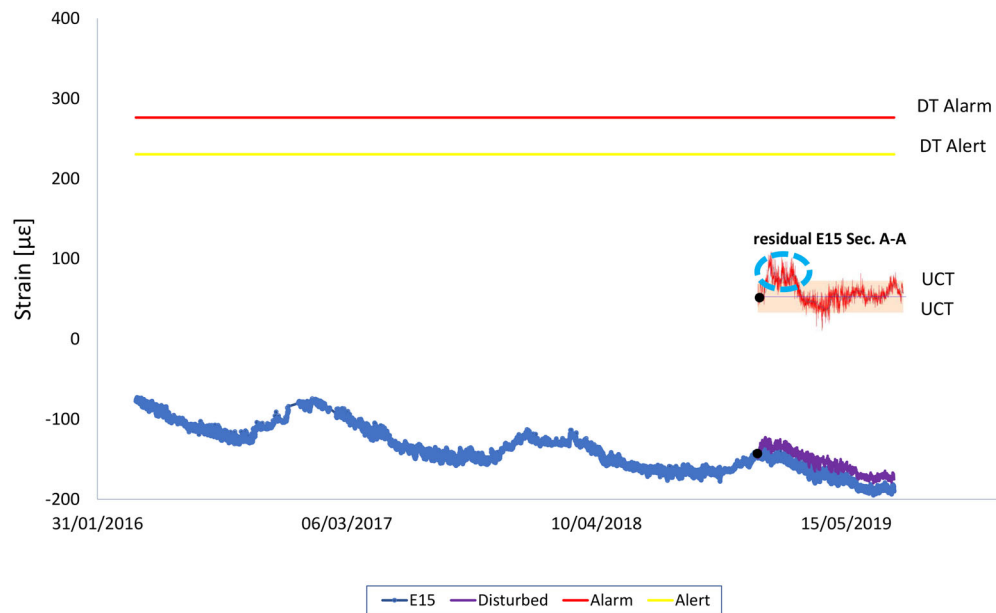
The data have been subjected to a data cleaning operation to remove outliers in the signals. An explanatory example has been reported in Figure 12. Furthermore, a pre-processing operation consisting in a z-score normalization w.r.t. the preceding 60 days, for input and output time-series, has been performed. Then, several regression models have been used, as in the previous case. Among them, those with the best results were the Extreme Gradient Boosting machine and Multi-Layer Perceptron, as in the previous case (the parameters characterizing such models are the same described in section 5.1.2). Actually, two sub-models associated to the Multi-Layer Perceptron, one for the transversal and

Table 4. Percentages of detected anomalies. Damage detection range definition: [80%, 100%], [40%, 80%], [0%–40%].

E10				E11			
Amplitude [$\mu\epsilon$]	Peak reach time [h]			Amplitude [$\mu\epsilon$]	Peak reach time [h]		
	168	336	720		168	336	720
2	0%	0%	0%	2	0%	0%	0%
10	53%	46%	40%	10	100%	80%	67%
15	93%	80%	60%	15	100%	100%	100%
20	100%	100%	87%	20	100%	100%	100%

E12				E15			
Amplitude [$\mu\epsilon$]	Peak reach time [h]			Amplitude [$\mu\epsilon$]	Peak reach time [h]		
	168	336	720		168	336	720
2	0%	0%	0%	2	0%	0%	0%
10	100%	100%	87%	10	93%	87%	73%
15	100%	100%	100%	15	100%	100%	93%
20	100%	100%	100%	20	100%	100%	100%

Damage detection colours definition: green, yellow, red.

**Figure 11.** Design thresholds (DT) and undamaged conditions thresholds (UCT).**Table 5.** Input and output parameters for correlation model.

INPUT	OUTPUT
Mean air temperatures = mean [T1, T2, T3]	MGB1L or MGB1T
CL1 CHB	
CL2 CHA	
CL2CHB	
Additional temporal features	

the other for the longitudinal sensor, have been used to fine-tune the results. The adoption of different parameter settings for the two sensors reflects their different nature. Such two sub-models are characterized by different values of two hyperparameters: the learning rate and the maximum number of epochs. The two mentioned hyperparameters have been set equal to 0.001 and 400 and to 0.002 and 100, respectively. Once used the regression model, the data have been rescaled with an inverse z-score normalization (post-processing operation).

Table 6 presents the comparison between the two models (the respective sub-models of the MLP and the Extreme Gradient Boosting Machine) with better metrics. In this case

the Multi-Layer Perceptron achieves better results. Figure 13 shows the subdivision in train set (60%), validation error set (10%) and test anomaly set (30%) of the overall data set.

5.2.3. Simulation of anomalies and damage identification

The procedure to define the healthy condition error range, to simulate the anomalies and to verify the capacity to catch them in terms of percentages has been the same described and used in the Sections 4, 5.1.2., and 5.1.3. In this case, the value of k chosen to define the extremes of the healthy condition error range, namely the UCT, has been equal to 2.5 for MGB1T and equal to 3 for MGB1L. This is due to the capacity of the system to detect very small anomalies, despite a wider healthy condition error range that allows to avoid false positives. For this problem, for both sub-models used, zero false positives were found.

Table 7 depicts the outcomes in terms of percentages of detected anomalies as a function of their amplitude and of the time span. The results may reflect good, mediocre or

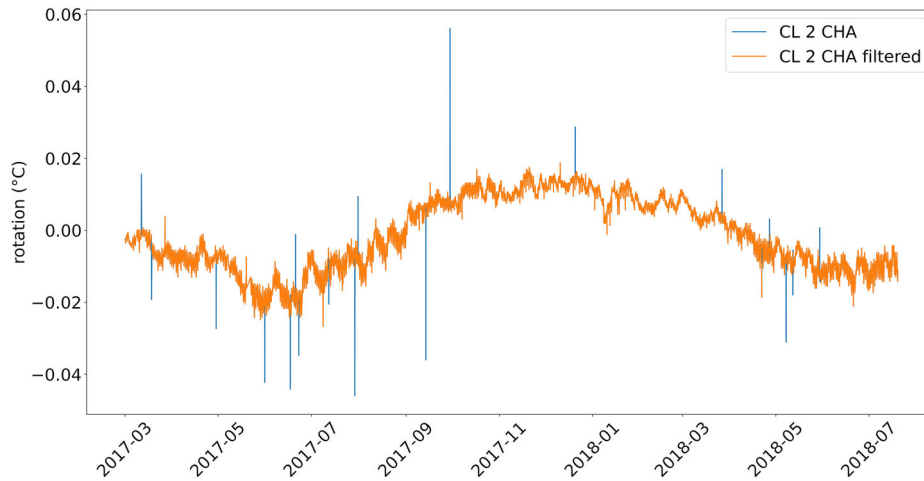


Figure 12. Longitudinal rotation CL2 CHA: original (blue) and filtered (orange) signal.

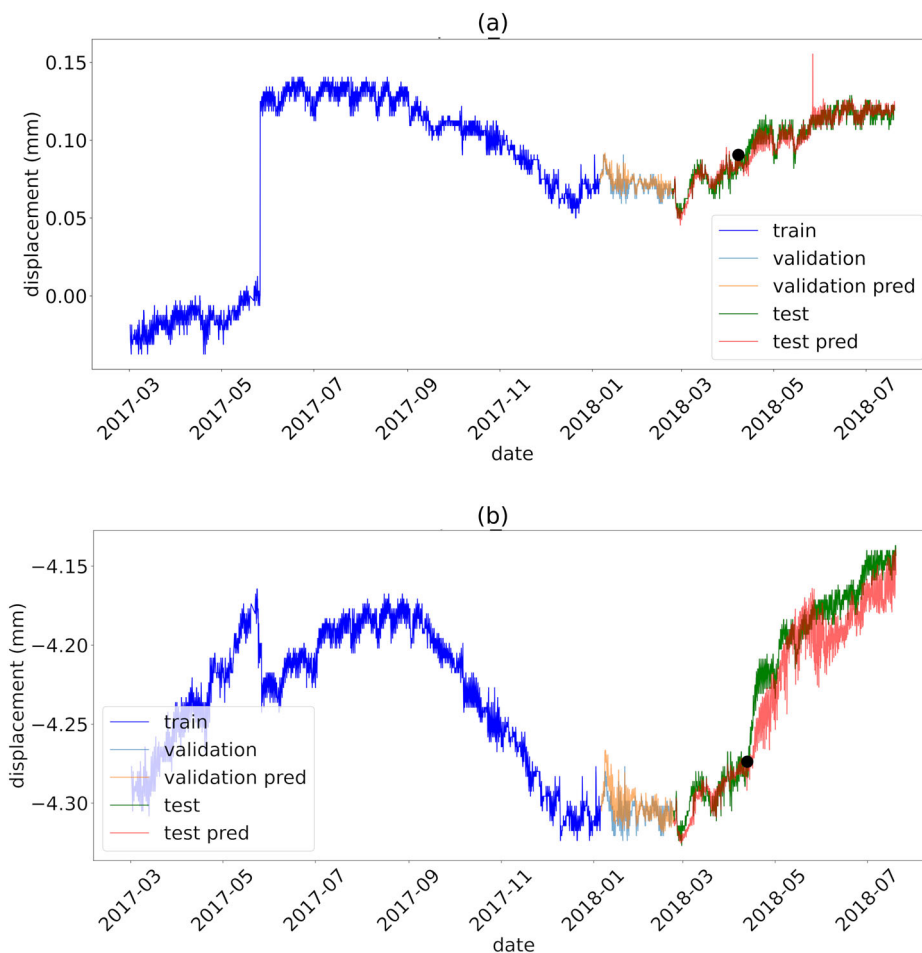


Figure 13. Displacements. Subdivision into train, validation error and test anomaly set. a Signals MGB1T; b Signal MGB1L.

Table 6. Models evaluation metrics (validation error set).

Sensor	MLP			XGBOOST		
	MAE (mm)	SMAPE (%)	R ² (-)	MAE (mm)	SMAPE (%)	R ² (-)
MGB1L	0.003	0.042	0.666	0.006	0.075	0.533
MGB1T	0.002	1.435	0.806	0.002	1.875	0.903

poor damage detection capacity. The range of percentages and the colour associated with each of these definitions is given in the table caption. The obtained outcomes, both for MGB1T and MGB1L, have been very satisfactory. MGB1T

Table 7. Percentage of detected anomalies (MGB1T and MGB1L). Damage detection range definition: [80%, 100%], [40%, 80%], [0%–40%].

Amplitude [mm]	MGB1T			MGB1L		
	Peak reach time [h]			Peak reach time [h]		
	168	336	720	168	336	720
0.005	60%	47%	0%	0.008	80%	80%
0.008	100%	100%	87%	0.01	100%	80%
0.01	100%	100%	87%	0.04	100%	100%

Damage detection colours definition: green, yellow, red.

shows good results from an anomaly with an amplitude of 0.008 mm, which is approximately 10% of the mean value of the signal. On the other hand, the damage detection capability using the MGB1L sensor is much greater as the results are already good for a 0.008 mm amplitude anomaly, which is equivalent to about 2 per thousand of the average signal. Even though the fault detection capacity has been considered reliable only for anomalies with an amplitude equal to or greater than 0.04 mm for MGB1L and 0.01 mm for MGB1T, it would turn out to be far greater than the one based on the design thresholds (DT). Indeed, the alert and alarm thresholds have been defined equal to ± 170.9 and ± 205 millimetres for MGB1L and to ± 60 and ± 72 millimetres for MGB1T. In this case the alert values for the design thresholds are the joint excursion values calculated in the two directions in the presence of an earthquake. The alarm thresholds are, as in the previous case, equal to 120% of these values.

6. Conclusions

This paper examines the static and environmental data recorded on a prestressed railway bridge in the first period of its service life. Correlation models have been developed following evaluations of cause-effect relationships between the measured quantities in the healthy condition. The modelling hypotheses underlying such correlations are based on physical phenomena. These last ones are described through relationships, linking input parameters (causes) to output ones (effects), which need to be expressed by articulated models given the structural complexity and the manifold of phenomena to which it is subject. In detail, two aspects have been investigated and controlled. The first one, the assessment of the midspan strain of the unloaded deck, has been addressed considering the influence of several factors. The temperature, its difference (gradient) measured over several distances, and other environmental factors (e.g. solar radiation) are among them. The second one, the assessment of pier rotations and joint expansion, has been accomplished by taking into account the influence of environmental parameters on such phenomena. The correlation characterizing the undamaged structural condition have been successfully modelled, providing very accurate predictions of the signal chosen as output of the model.

The addition of a pre-processing operation, consisting of a z-score normalization on a sliding window, has been shown a tool able to mitigate the effects due to both structural and non-structural deferred phenomena. This is essential to obtain repetitiveness in the data. Moreover, this enables to train effective correlation models and to derive the undamaged structural condition. On the other hand, the use of additional temporal parameters has been particularly effective in solving the lack of some environmental parameters like solar radiation. The followed signal analysis and reconstruction approach have led to the definition of undamaged-condition alarm thresholds (UCT) and to a successful fault detection that have overcome the results achievable with the traditional thresholds (DT) based on the

design values. Particular attention was focused on the reduction of false alarms. Their number was reduced using the moving median of the residual between the predicted and the measured signal as a damage index.

The choice of features composing the correlation models, the use of pre-processing operations to give repetitiveness to data over time, the exploitation of some temporal parameters to compensate for the shortage of some environmental parameters, the selection and the training of specific regression model, and the proposed damage index have been found to be very efficient. This case study can be a starting point to facilitate the assessment of railway bridges similar, in static scheme and geometry, to the investigated one. A continuous improvement for such analysed bridge would be done by means of new accumulated data in time, although the already satisfactory results. Moreover, the acquired knowledge could be used to investigate similar structures with less available data. Indeed, an advantage in developing such models is their future generalization to the analyzed structural typology that could be done with the introduction in this context of domain adaptation techniques (e.g. Wang, Michau, & Fink, 2019) already performed successfully to address other issues in civil engineering (e.g. Gopalakrishnan, Gholami, Vidyadharan, Choudhary, & Agrawal, 2018; Yang, Shi, Chen, & Lin, 2020; Zhu, Zhang, Qi, & Lu, 2020, Chiaia, Marasco, & Aiello, 2022).

Disclosure statement

No potential conflict of interest was reported by the authors.

ORCID

Giulia Marasco  <http://orcid.org/0000-0002-5264-8947>
 Bernardino Chiaia  <http://orcid.org/0000-0002-5469-2271>
 Giulio Ventura  <http://orcid.org/0000-0001-5464-6091>
 Fabrizio Dominici  <http://orcid.org/0000-0001-8584-3071>
 Claudio Rossi  <http://orcid.org/0000-0001-5038-3597>

References

- Al Shalabi, L., Shaaban, Z., & Kasasbeh, B. (2006). Data mining: A pre-processing engine. *Journal of Computer Science*, 2(9), 735–739.
- Al-Dahidi, S., Baraldi, P., Di Maio, F., & Zio, E. (2014). Quantification of signal reconstruction uncertainty in fault detection systems. In *PHM Society European Conference*.
- Arul, M., & Kareem, A. (2020). Data anomaly detection for structural health monitoring of bridges using shapelet transform. arXiv Preprint arXiv:2009.00470.
- Avci, O., Abdeljaber, O., Kiranyaz, S., Hussein, M., Gabbouj, M., & Inman, D. J. (2021). A review of vibration-based damage detection in civil structures: From traditional methods to Machine Learning and Deep Learning applications. *Mechanical Systems and Signal Processing*, 147, 107077. doi:10.1016/j.ymssp.2020.107077
- Azzara, R. M., De Falco, A., Girardi, M., & Pellegrini, D. (2017). Ambient vibration recording on the Maddalena Bridge in Borgo a Mozzano (Italy): Data analysis. *Annals of Geophysics*, 60(4). doi:10.4401/ag-7159
- Bao, Y., Chen, Z., Wei, S., Xu, Y., Tang, Z., & Li, H. (2019). The state of the art of data science and engineering in structural health monitoring. *Engineering*, 5(2), 234–242. doi:10.1016/j.eng.2018.11.027

- Bao, Y., & Li, H. (2021). Machine learning paradigm for structural health monitoring. *Structural Health Monitoring*, 20(4), 1353–1372. doi:10.1177/1475921720972416
- Bień, J., Jakubowski, K., Kamiński, T., Kmita, J., Kmita, P., Cruz, P. J. S., & Maksymowicz, M. (2007). Railway bridge defects and degradation mechanisms.
- Cardini, A. J., & DeWolf, J. T. (2009). Long-term structural health monitoring of a multi-girder steel composite bridge using strain data. *Structural Health Monitoring*, 8(1), 47–58. doi:10.1177/1475921708094789
- Chen, T., & Guestrin, C. (2016). Xgboost: A scalable tree boosting system. In *Proceedings of the 22nd ACM SIGKDD International Conference on Knowledge Discovery and Data Mining*.
- Chiaia, B., Marasco, G., & Aiello, S. (2022). Deep convolutional neural network for multi-level non-invasive tunnel lining assessment. *Frontiers of Structural and Civil Engineering*, 16(2), 214–223. doi:10.1007/s11709-021-0800-2
- Chiaia, B., Marasco, G., Ventura, G., & Zannini Quirini, C. (2020). Customised active monitoring system for structural control and maintenance optimisation. *Journal of Civil Structural Health Monitoring*, 10(2), 267–282. doi:10.1007/s13349-020-00382-8
- Chiaia, B., Ventura, G., Zannini Quirini, C., & Marasco, G. (2019). Bridge active monitoring for maintenance and structural safety. In *International Conference on Arch Bridges* (pp. 866–873). Springer.
- Chou, J. H., & Ghaboussi, J. (2001). Genetic algorithm in structural damage detection. *Computers & Structures*, 79(14), 1335–1353. doi:10.1016/S0045-7949(01)00027-X
- Civera, M., Zanotti Fragonara, L., & Surace, C. (2020). An experimental study of the feasibility of phase-based video magnification for damage detection and localisation in operational deflection shapes. *Strain*, 56(1), e12336. doi:10.1111/str.12336
- Ding, Y. L., Wang, G. X., Sun, P., Wu, L. Y., & Yue, Q. (2015). Long-term structural health monitoring system for a high-speed railway bridge structure. *TheScientificWorldJournal*, 2015, 250562. doi:10.1155/2015/250562
- Duan, Y.-F., Li, Y., & Xiang, Y.-Q. (2011). Strain-temperature correlation analysis of a tied arch ridge using monitoring data. In *International Conference on Multimedia Technology*.
- Gonzales, I., Ülker-Kaustell, M., & Karoumi, R. (2013). Seasonal effects on the stiffness properties of a ballasted railway bridge. *Engineering Structures*, 57, 63–72. doi:10.1016/j.engstruct.2013.09.010
- Gopalakrishnan, K., Gholami, H., Vidyadharan, A., Choudhary, A., & Agrawal, A. (2018). Crack damage detection in unmanned aerial vehicle images of civil infrastructure using pre-trained deep learning model. *International Journal of Traffic and Transportation Engineering*, 8(1), 1–14.
- Guo, T., Sause, R., Frangopol, D. M., & Li, A. (2011). Time-dependent reliability of PSC box-girder bridge considering creep, shrinkage, and corrosion. *Journal of Bridge Engineering*, 16(1), 29–43. doi:10.1061/(ASCE)BE.1943-5592.0000135
- Hu, Y., Palmé, T., & Fink, O. (2017). Fault detection based on signal reconstruction with auto-associative extreme learning machines. *Engineering Applications of Artificial Intelligence*, 57, 105–117. doi:10.1016/j.engappai.2016.10.010
- Inaudi, D. (2010). Long-term static structural health monitoring. In *Structures Congress* (pp. 566–577).
- Ivanovic, S. S., Trifunac, M. D., & Todorovska, M. I. (2000). Ambient vibration tests of structures—a review. *ISSET Journal of Earthquake Technology*, 37(4), 165–197.
- Jenkins, C. H., Kjerengtroen, L., & Oestensen, H. (1997). Sensitivity of parameter changes in structural damage detection. *Shock and Vibration*, 4(1), 27–37. doi:10.1155/1997/807239
- Kamaitis, Z., & Kamaitis, Z. (1996). The causes of shear cracking in prestressed concrete box-girder bridges. *Statyba*, 2(8), 26–34. doi:10.1080/13921525.1996.10590169
- Li, S., Yang, Y., Pu, Q., Yang, D., Sun, B., & Li, X. (2019). Three-dimensional nonlinear creep and shrinkage effects of a long-span prestressed concrete box girder bridge. *Structural Concrete*, 20(2), 638–649. doi:10.1002/suco.201800148
- Liu, G., Niu, Y., Zhao, W., Duan, Y., & Shu, J. (2022). Data anomaly detection for structural health monitoring using a combination network of GANomaly and CNN. *Smart Structures and Systems*, 29(1), 53–62.
- Liverani, R. (n.d.). *Analisi delle deformazioni di un ponte a travata continua in cemento armato* [Doctoral dissertation].
- Magalhães, F., & Cunha, A. (2011). Explaining operational modal analysis with data from an arch bridge. *Mechanical Systems and Signal Processing*, 25(5), 1431–1450. doi:10.1016/j.ymssp.2010.08.001
- Magalhães, F., Cunha, A., & Caetano, E. (2009). Online automatic identification of the modal parameters of a long span arch bridge. *Mechanical Systems and Signal Processing*, 23(2), 316–329. doi:10.1016/j.ymssp.2008.05.003
- Marasco, G., Piana, G., Chiaia, B., & Ventura, G. (2022). Genetic algorithm supported by influence lines and neural network for bridge health monitoring. *Journal of Structural Engineering*, 148(9), 04022123. doi:10.1061/(ASCE)ST.1943-541X.0003345
- Matsuoka, K., Tokunaga, M., & Kaito, K. (2021). Bayesian estimation of instantaneous frequency reduction on cracked concrete railway bridges under high-speed train passage. *Mechanical Systems and Signal Processing*, 161, 1–26.
- McClelland, J. L., Rumelhart, D. E., & Hinton, G. E. (1986). *The appeal of parallel distributed processing*. Cambridge, MA: MIT Press.
- Nawi, N. M., Atomi, W. H., & Rehman, M. Z. (2013). The effect of data pre-processing on optimized training of artificial neural networks. *Procedia Technology*, 11, 32–39. doi:10.1016/j.protcy.2013.12.159
- Nguyen, V. H., Schommer, S., Maas, S., & Zürbes, A. (2016). Static load testing with temperature compensation for structural health monitoring of bridges. *Engineering Structures*, 127, 700–718. doi:10.1016/j.engstruct.2016.09.018
- Obaid, H. S., Dheyab, S. A., & Sabry, S. S. (2019). The impact of data pre-processing techniques and dimensionality reduction on the accuracy of machine learning. In *2019 9th Annual Information Technology, Electromechanical Engineering and Microelectronics Conference*. IEEE (pp. 279–283).
- Ogasawara, E., Martinez, L. C., De Oliveira, D., Zimbrão, G., Pappa, G. L., & Mattoso, M. (2010). Adaptive normalization: A novel data normalization approach for non-stationary time series. In *2010 International Joint Conference on Neural Networks*. IEEE.
- Peeters, B., & De Roeck, G. (2001). One-year monitoring of the Z24-Bridge: Environmental effects versus damage events. *Earthquake Engineering & Structural Dynamics*, 30(2), 149–171. doi:10.1002/1096-9845(200102)30:2<149::AID-EQE1>3.0.CO;2-Z
- Priori, C., De Angelis, M., & Betti, R. (2018). On the selection of user-defined parameters in data-driven stochastic subspace identification. *Mechanical Systems and Signal Processing*, 100, 501–523. doi:10.1016/j.ymssp.2017.07.045
- Quinlan, J. R. (1986). Induction of decision trees. *Machine Learning*, 1(1), 81–106. doi:10.1007/BF00116251
- Rainieri, C., & Fabbrocino, G. (2010). Automated output-only dynamic identification of civil engineering structures. *Mechanical Systems and Signal Processing*, 24(3), 678–695. doi:10.1016/j.ymssp.2009.10.003
- Roselli, I., Malena, M., Mongelli, M., Cavalagli, N., Gioffrè, M., De Canio, G., & de Felice, G. (2018). Health assessment and ambient vibration testing of the “Ponte delle Torri” of Spoleto during the 2016–2017 Central Italy seismic sequence. *Journal of Civil Structural Health Monitoring*, 8(2), 199–216. doi:10.1007/s13349-018-0268-5
- Sanayei, M., Phelps, J. E., Sipple, J. D., Bell, E. S., & Brenner, B. R. (2012). Instrumentation, nondestructive testing, and finite-element model updating for bridge evaluation using strain measurements. *Journal of Bridge Engineering*, 17(1), 130–138. doi:10.1061/(ASCE)BE.1943-5592.0000228
- Sgambi, L., Malerba, P. G., Gotti, G., & Ielmini, D. (2012). The influence of degradation phenomena on collapse modes in prestressed concrete beams. *International Journal of Lifecycle Performance Engineering*, 1(1), 41–63. doi:10.1504/IJLCP.2012.051280
- Tang, Z., Chen, Z., Bao, Y., & Li, H. (2019). Convolutional neural network-based data anomaly detection method using multiple

- information for structural health monitorin. *Structural Control and Health Monitoring*, 26(1), e2296. doi:10.1002/stc.2296
- Tonnoir, B., Carde, C., & Banant, D. (2018). Curvature: An Indicator of the mechanical condition of old prestressed concrete bridges. *Structural Engineering International*, 28(3), 357–361. doi:10.1080/10168664.2018.1490585
- Tsay, R. S. (2005). *Analysis of financial time series*. John Wiley & Sons.
- Wang, Q., Michau, G., & Fink, O. (2019). Domain adaptive transfer learning for fault diagnosis. In *2019 Prognostic and System Health Management Conference (PHM-Paris)*, pp. 279–285.
- Wu, C., Wu, P., Wang, J., Jiang, R., Chen, M., & Wang, X. (2022). Critical review of data-driven decision-making in bridge operation and maintenance. *Structure and Infrastructure Engineering*, 18(1), 47–70. doi:10.1080/15732479.2020.1833946
- Yang, Q., Shi, W., Chen, J., & Lin, W. (2020). Deep convolution neural network-based transfer learning method for civil infrastructure crack detection. *Automation in Construction*, 116, 103199. doi:10.1016/j.autcon.2020.103199
- Zhang, Z., Yan, J., Li, L., Pan, H., & Dong, C. (2021). Condition assessment of stay cables through enhanced time series classification using a deep learning approach. arXiv Preprint arXiv:2101.03701.
- Zhou, G.-D., & Yi, T.-H. (2014). A summary review of correlations between temperatures and vibration properties of long-span bridges. *Mathematical Problems in Engineering*, 2014, 1–19. doi:10.1155/2014/638209
- Zhu, J., Zhang, C., Qi, H., & Lu, Z. (2020). Vision-based defects detection for bridges using transfer learning and convolutional neural networks. *Structure and Infrastructure Engineering*, 16(7), 1037–1049. doi:10.1080/15732479.2019.1680709